Comparison between the role of discontinuities in cardiac conduction and in a one-dimensional hardware model

M. deCastro,[1],* E. Hofer,[2] A. P. Muñuzuri,[1] M. Gómez-Gesteira,[1] G. Plank,[2] I. Schafferhofer,[2] V. Pérez-Muñuzuri,[1] and V. Pérez-Villar[1]

[1]*Grupo de Fisica No Lineal, Facultad de Fisica, Universidad Santiago de Compostela, 15706 Santiago de Compostela, Spain*
[2]*Institut für Medizinische Physik und Biophysik, Karl-Franzens-Universität, A-8010 Graz, Austria*

In real electrophysiological experiments, irregularities in the extracellular excitation spread are believed to depend on cardiac tissue microstructure. An electronic hardware model was developed to analyze this dependence by placing some inhomogeneities (slow propagation areas) in the medium. The position of such inhomogeneities is correlated with abnormal delays and irregularities measured in signal propagation. [S1063-651X(99)10505-1]

I. INTRODUCTION

Discrete and continuous nonlinear models have been widely used as standard models to simulate the excitation spread in many different systems in nature; i.e., transformation and transport processes in living cells, tissues, neuron networks, physiological systems and ecosystems, as well as in all forms of chemical and biochemical reactions and combustion systems [1–6]. This technique has been applied to describe the normal and abnormal excitation spread in the heart and some phenomena of arrhythmias like reentry and fibrillation [7,8].

The mechanisms of normal as well as abnormal conduction in the heart can be seen from different levels of scaling. At a large scale (mm) normal cardiac tissue behaves like a continuous anisotropic active medium (syncytium). However, in the cellular and subcellular range, <120 μm, we know that the tissue consists of a discretely coupled network of excitable units (cells) with cylinderlike geometry. The individual cells are connected electrically by conductive pores called gap junctions [9–12]. Gap junctions are not equally distributed at the cell surface [13]. At some sites, this coupling can be diminished by a lower density of gap junctions or a complete loss of intercellular coupling can be found if the space between cells is invaded by connective tissue or microvessels. Some heterogeneity in microstructure is also present in normal tissue but in case of microfibrosis it is substantially increased. Microfibrosis is a microstructural disease, which can be found in hypertrophy, in zones of healed infarctions and in aging hearts.

During *in vitro* experiments, cardiac tissue is surrounded by a solution of electrolytes (Tyrode's solution) that reproduces the extracellular fluid and has a specific conductivity of 19.2 mS/cm. In this way an electrical discretely coupled active medium (tissue) is interfaced to a continuous passive medium (volume conductor). Local excitation processes associated with cellular inward currents generate electrical fields in the volume conductor which can be measured as *extracellular* potentials Φ_e. By means of sensors with multiple electrodes placed in the volume conductor, the distribution of potentials during the excitation spread can be recorded. During the activation process (depolarization) the typical extracellular signal shows a smooth biphasic waveform. However, electrograms recorded at the surface of cardiac tissue often look slightly or severely distorted (fractionated electrograms). Such *fractionated electrograms* have been measured at sites of local conduction disturbance or conduction block [14–16]. The question arises if these irregularities reflect discontinuous conduction due to microstructural discontinuities of the tissue and spatially complex pathways of the propagating wave induced by these disturbances. During the *in vitro* experiment, the detailed topology of the coupling network within the tissue under study cannot be determined. Since these sites of uncoupling are not known *a priori*, fractionated electrograms with multiple deflections are difficult to interpret.

Since the beginning of this decade, the use of nonlinear circuits has constituted a powerful tool for studying diverse phenomena related to wave propagation in active media [17–23]. In particular, arrays of such circuits provide an electronic model well suited for simulation of processes of cardiac conduction, since one can control both the elements and the connections among them.

In our experiments, an electronic simulator (a one-dimensional array of nonlinear electronic circuits) [24,25] was built with two different types of connections among electronic units, a one-to-one purely diffusive (resistive) coupling between consecutive circuits and a global coupling by shunting every circuit of the chain via a passive volume conductor. This setup allows one to control the degree of coupling between neighboring circuits at specific sites and to study how signals in the volume conductor as well as in the excitable array are affected by this procedure.

The aim of this paper is (1) to describe, by this electronic simulator, the basic mechanisms of propagation disturbances induced by local discontinuities of coupling in the active discrete medium and (2) to compare these findings with results from *in vitro* experiments showing fractionated electro-

---

*Author to whom correspondence should be addressed. Electronic address: uscfmmcr@cesga.es

grams which may be produced by the microscopic obstacles in the cardiac tissue.

II. METHODS

A. Electrophysiological experiments

Isolated cardiac strands, with cablelike geometry (papillary muscle) removed from the hearts of guinea pigs and placed in a tissue bath and superfused with oxygenated Tyrode's solution ([mM/l] NaCl 132.1, KCl 5.4, CaCl$_2$ 2.5, MgCl$_2$ 1.15, NaHCO$_3$ 24, NaH$_2$PO$_4$ 0.42 and D-glucose 5.6, pH 7.35) at 36.5 °C. The preparation was stimulated at its surface by an unipolar electrode with electrically isolated constant current pulses of 1 ms duration and twice the threshold strength.

Extracellular signals were recorded with transparent microminiature electrode arrays, which could be positioned accurately at given sites and distances related to the surface of the preparation by means of a custom designed 3D micromanipulator. The distance between the recording array and the surface of the preparation was kept at 20 to 50 μm on one hand, in order to be as close as possible to the local current source of the tissue and on the other hand, to prevent hypoxia effects induced by obliteration of the flow of superfusate. Due to the lack of any attachment procedure and due to the fact that during the phase of activation under study contraction has not started yet, motion artifacts were negligible. The sensor array contained 25 electrodes of two-dimensional arrangements according to the type of the array. Interelectrode spacing was 50 μm (center to center). This is less than the average length of a cell and covers the range of the expected size of recurrent microstructural discontinuities of the tissue. Data were acquired with a 24-channel transient recorder (Krentz TR6400) at 200 kHz sampling rate and 12 bits vertical resolution each channel. Data then were transferred to a UNIX based computer (SUN IPX) running a custom designed database for electrophysiological experiments. A detailed description of the recording technique is given in [26]. The sketch of this setup is depicted in Fig. 1.

Longitudinal propagation (LP) parallel to the fiber axis is expected to be faster than transverse (TP) to its axis [27,28]. This macroscopic effect of anisotropy of conduction reflects the influence of the average density of gap junctions, which is lower side by side than at the front ends of the cylindrical shaped cells. At a microscopic size scale, not only the average density of junctions, but also the spatial distribution might become important. Due to fewer side to side coupling of cells we expect to find increased discontinuities in propagation during TP. In experiments we induced LP and TP by changing the site of the stimulus and keeping the recording sites constant (Fig. 1). From the depolarization signal Φ_e, which lasts a couple of milliseconds, some authors [29] have shown that the negative peak of its first time derivative, $d\Phi_e/dt$, can be used as a specific time marker to determine the local activation time (LAT). At sites of multiple deflections of $d\Phi_e/dt$, multiple LATs were computed. The spatial course of LAT, local conduction velocity and amplitude of $d\Phi_e/dt$ was evaluated in order to describe the dynamical electrical patterns of continuous and discontinuous excitation spread.
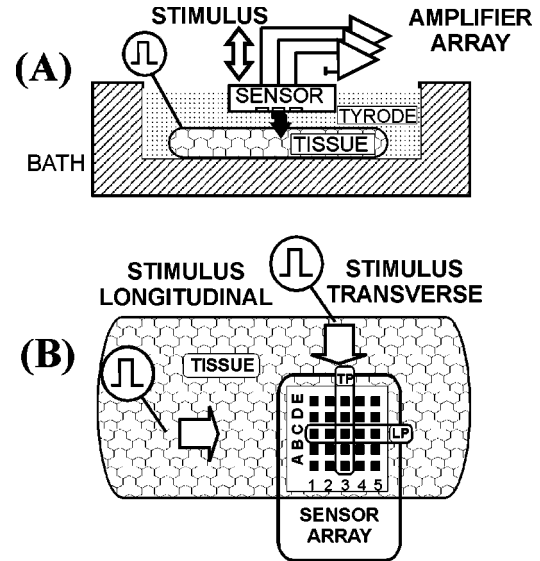

FIG. 1. (a) Sectional view of the experimental setup for *in vitro* studies. The sensor as well as amplifiers are carried out for 25 channels. The cablelike tissue (papillary muscle) was mounted in the bath filled with conductive fluid (Tyrode's solution). A pointlike stimulus was set at specific sites of the preparation to induce a propagating wave of excitation. (b) Top view of the experimental procedure. The position of the electrode array with matrixlike electrode arrangements was kept constant. The direction longitudinal (LP) and transverse (TP) to the fiber axis was obtained by changing the stimulus site.

B. Electronic simulator

The electronic model (1D array of electronic circuits) has been chosen to mimic and interpret some propagation phenomena previously found in real cardiac tissue. A 1D chain of electronic circuits is connected via a network of resistances together. This network is interfaced to a 2D like volume conductor (see Fig. 2). In this way, our model is a quasi-2D model of excitation spread, which represents the behavior of discretely coupled excitable units interfaced to a passive and continuous volume conductor, rather than to reproduce the biophysical behavior of the tissue.

The electronic simulator (Fig. 2) consists of a linear array of 30 Chua circuits embedded in a continuous and passive volume conductor. A Chua's circuit is a nonlinear circuit [24,25], which works in an excitable state with the set of parameters shown in Table I. Initially, all these circuits were adjusted to have the same initial stable state within the tolerances allowed commercially. Two different connections among circuits were considered; namely, an internal (resistive) one-to-one coupling and an external (global) coupling.

Every circuit in the array was connected to its nearest neighbors by resistances $R_{\text{int}}=4.7$ kΩ to form a one-dimensional cable [21]. These resistances were replaced at a specific site (between circuits 21 and 23) by resistors, R_a, to decrease the coupling between circuits and produce propagation failure [30,31].

The external coupling was achieved by connecting every circuit in the array (nodes $A_1 \ldots A_{30}$) to an external passive medium (nodes $C_1 \ldots C_{30}$) by resistances $R_e=1$ kΩ as shown in Fig. 2. The external medium was formed by a Plexiglas container 52 cm long, 45 cm wide and 1 cm deep,
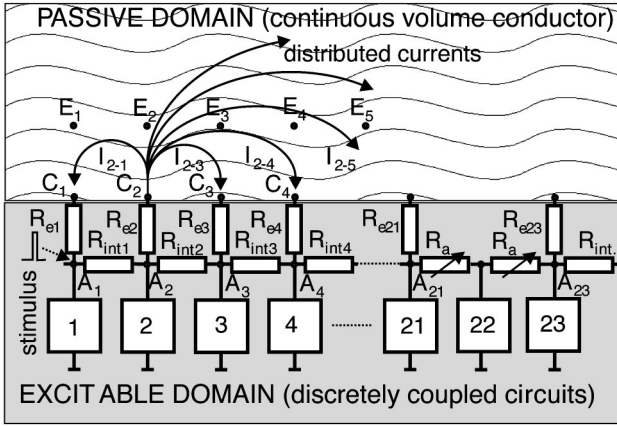
FIG. 2. Electronic experimental setup. The excitable medium is formed by an array of electronic units (Chuas circuits, 1, 2, 3, ...) which are coupled one to one by resistors (R_{int1}, R_{int2}, R_{int3}...). Velocity of excitation spread is controlled by this coupling. Local change or even block of propagation can be induced by setting the coupling resistors of a specific circuit (22) to high values R_a. The signals of the individual circuit outputs (measured at nodes A_i) are led to connector terminals C_i via resistors (R_{ei}) and interfaced to the passive volume conductor. This yields a spatial distribution of currents flowing from an individual terminal C_i to the other terminals, ... C_{i-1}, C_{i+1}, C_{i+2} ... similar to the "local current mechanisms" postulated by physiologists in propagating biosignals. Signals within the volume conductor (V_e) can be measured at positions E_i which reflect a fixed distance from the current outputs (C_i) and specific sites along the axis of propagation (index I of the circuits). An electrical stimulus pulse was applied at node A_i.

which was filled up with distilled water (conductivity 3μS/cm). The distance between two consecutive circuit outputs connected to the bath was 0.9 cm, except between circuits 21–23, where it was 1.8 cm. The terminal of circuit 22 was isolated from the volume conductor to enhance the effect of that abnormal site on wave propagation. The values of R_a and R_e corresponding to the abnormal coupling site (ACS from now on) are summarized in Table II. Their commercial tolerance was 1%.

The effect of this ACS on the spread of excitation can be measured at internal nodes $A_1 \ldots A_{30}$ or at external nodes $E_1 \ldots E_{30}$ embedded into the conductive volume and placed 0.9 cm far from connection points $C_1 \ldots C_{30}$. To produce an excitation wave spreading in this medium, a pulse was delivered at the first circuit of the array by a wave form generator (Hewlett-Packard 33120A) with a constant amplitude of 3.5 V and a pulse width of 20 μs. Circuits were sampled with a digital oscilloscope (Hewlett-Packard 54601) with a sampling rate of 4 MHz and 8 bits A/D resolution.

TABLE I. Set of parameters corresponding to each Chua's circuit in the array.

Parameters	Tolerances (%)	Nonlinear components
$C_1 = 1$ nF	5	$G_1 = 3.81 \times 10^{-3}$ Ω^{-1}
$C_2 = 100$ nF	5	$G_2 = 3.70 \times 10^{-3}$ Ω^{-1}
$L = 10$ mH	10	$G_0 = -4.56 \times 10^{-3}$ Ω^{-1}
$R = 270$ Ω	1	

TABLE II. Resistive values at the ACS.

Array position	R_a (kΩ)	R_e (kΩ)
21-22	10.0	1
22		No connection
22-23	1.0	1

Data were acquired by this oscilloscope and stored in a personal computer.

Our particular choice of circuitry has a series of advantages and limitations. Most of the models of excitation spread [32] consider intracellular axial resistance, and membrane properties, but neglect the resistance formed by extracellular volume conductor (which is assumed to be shortcutted). In contrast, our model deals specifically with the distribution of local current in the volume conductor, which is also applied in reality. On the other hand, the existence of R_e between nodes C and A allows one to measure the local current flowing into volume conductor without changing the conductivity of the bath, since $R_e = 1$ kΩ is much smaller than the liquid resistance, $R \approx 300$ kΩ. Nevertheless, our electronic model has some important limitations, for example, we have considered a common ground for all circuits. To reproduce the nature of cardiac tissue, it would be necessary to build a separate ground as well as a power supply for each circuit, which is far beyond our technical availabilities. In summary, the hardware model does not pretend to reproduce the complexity of a real system as cardiac tissue, it only mimics some of its conduction properties at a microscopic level.

III. RESULTS

A. *In vitro* experiments

Wave forms of normal extracellular depolarization signals Φ_e are biphasic and smooth in shape [see Fig. 3(a)]. Amplitudes (peak to peak) of between 2 and 50 mV can be expected depending on the species, on the type of preparation and on the distance between the electrode array and the surface of the tissue. The duration of the signal is hard to de-
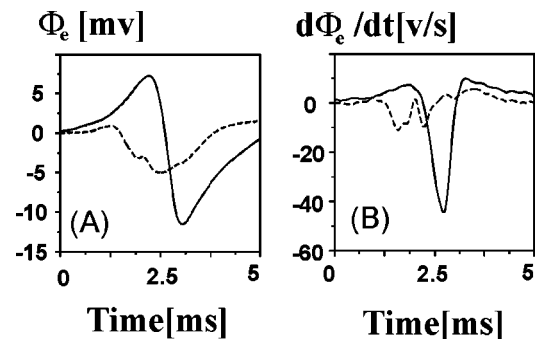

FIG. 3. (a) Typical extracellular depolarization signals (Φ_e) of longitudinal propagation (solid line) and transverse propagation (dashed line), recorded close to the surface of the tissue. The corresponding derivatives ($d\Phi_e/dt$) are depicted in (b). The distance of the recording array to the surface was usually kept to 20 -50 μm. Values in amplitude of Φ_e and of $d\Phi_e/dt$ at a given distance can vary from preparation to preparation.

termine because of the slow initial and ending phase, but the time span between the maximum and the minimum of the signal Φ_e gives a good measure for the duration of the depolarization process. This value is in the range of 1 ms and less. The derivative $d\Phi_e/dt$ of the extracellular signal Φ_e is triphasic [Fig. 3(b)] with a large negative peak deflection $d\Phi_e/dt_{peak}$ of typically 20–80 V/s during LP. This type of electrogram allows the determination of a distinct value of time by taking the instant of the negative peak derivative for LAT.

Electrograms arising from excitation spread transverse to the fiber axis (TP) differ in shape and amplitude [Fig. 3(a), dashed line]. Amplitudes decrease substantially, the shape of wave form appears distorted and the duration of the depolarization process was increased (by a factor of 2 and larger). The altered shape of $d\Phi_e/dt$ [Fig. 3(b)] enhances the character of fractionation and illustrates that multiple, at least two, processes of local depolarization take place during TP.

Isochrone maps obtained from 200×200 μm^2 of tissue during LP [Fig. 4(a)] indicate quite uniform propagation with an average velocity of 0.49 m/s. In contrast to this, TP at the same recording site resulted in substantial irregularities of wave fronts [Fig. 4(b)] and large changes of local conduction velocities (1:10). Average conduction velocity was estimated with 0.2 m/s. In order to follow the spatio-temporal relationship of $d\Phi_e/dt$ in normal electrograms [Fig. 4(d)], we recorded five extracellular signals at interelectrode distances of 50 microns [signals from site 1 to 5, row C of the array; see Fig. 1(b)]. The waterfall plot of these five signals indicates continuous conduction without any irregularities in shape of $d\Phi_e/dt$ or in delay between neighboring recordings. Values of $d\Phi_e/dt_{peak}$ were between 63 and 67 V/s.

During TP of the cardiac impulse (recordings taken at electrodes A to E from the second column of the array) the spatio-temporal relationship of $d\Phi_e/dt$ became quite complex [Fig. 4(d)]. In summary, we found several piecewise propagating events (indicated by a plausible delay of signals from neighboring recording sites) which ended in electrotonic behavior. Electrotonic means that the signal is not propagating in the excitable medium. In the volume conductor delays of those signals taken at different sites are negligible and their amplitude decreases with distance to the signal source. From the electrograms showing multiple deflections, three piecewise propagating waves could be detected [marked in Fig. 4(d) with encircled numbers 1, 2 and 3]. Wave 1, which enters from site E, seems to stop in D. This is indicated by the same LAT (4.88 ms) and by the decreasing amplitude at site C. At B and A, this signal disappears. Wave 2, is represented in all signals ($E-A$) but is propagating only between D and B. Wave 3 seems to start propagation in A.

B. Electronic simulator

Figure 5(a) shows the external signal with (thicker line) and without (thinner line) abnormal sites measured at E_{23} (see Fig. 2) . The first time derivative of that external signal dV_e/dt is shown in Fig. 5(b). Note that the external signal at ACS is more complex. From now on, we will use both the depolarization wave (first part of the biphasic activation process) and its first time derivative to determine the LAT.
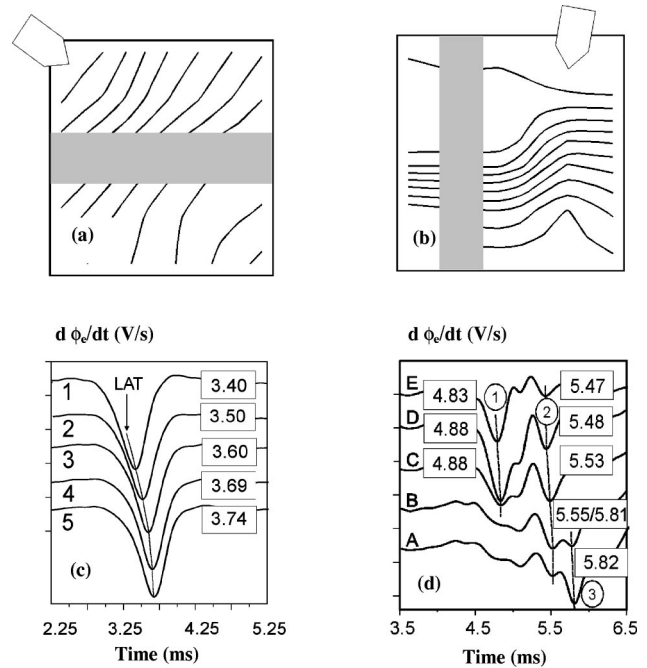

FIG. 4. (a) Isochrone map of propagation longitudinal to the fiber axis (LP). The isochrone interval is 50 μs. The total area of recording is 200×200 μm; the shaded area indicates the subset of recordings taken for signal analysis of LP. (b) Isochrone map of propagation transverse to fiber axis (TP) taken at same site as in (a). The isochrone interval is 100 μs. The shaded area indicates the subset of recordings taken for signal analysis of TP. (c) $d\Phi_e/dt$ during LP taken from five neighboring recording sites [electrodes 1, 2, 3, 4 and 5 from row C of the array; see shaded area in (a)], separated by 50 μm. The local activation time (ms) of each recording site is quoted in rectangular symbols. Its spatiotemporal course is marked by a dashed line. Vertical tick mark intervals correspond to 25 V/s. (d) Complex signals of transverse propagation. $d\Phi_e/dt$ from five neighboring sites [electrodes E, D, C, B, and A of column 2 of the array; see shaded area in (b)], separated by 50 μm. The course of the 3 major waves of activation (marked with encircled numbers 1, 2, and 3), is indicated by dashed lines. The corresponding activation times (ms) are quoted in rectangular symbols placed on the signal. Vertical tick mark intervals correspond to 10 V/s.

The internal depolarization signal (V_i) and its first time derivative (dV_i/dt) around the region of abnormal propagation (from circuits 17 to 27) are shown in Fig. 6(a) and 6(b). The shape and amplitude of every signal and its derivative are independent of the distance to the ACS. Only small differences were observed (less than 5%) in signal amplitude due to commercial tolerance of components in each individual Chua's circuit. In Fig. 6(a) internal signal (V_i) of consecutive recording points (circuits 17 to 21 and 23 to 27) are depicted. Equal delays corresponding to a constant conduction velocity of 0.14 circuits/μs are observed for circuits far from ACS. Note that the delay between two neighboring circuits was 7.0 μs but, the delay between circuits 21 and 23 was 25.2 μs instead of expected 14.0 μs, which indicates an additional delay generated by the ACS. The same behavior can be observed in Fig. 6(b) regarding the first time derivative (dV_i/dt).

The external depolarization signal (V_e) and its first time derivative (dV_e/dt) around the ACS are shown in Figs. 7(a)
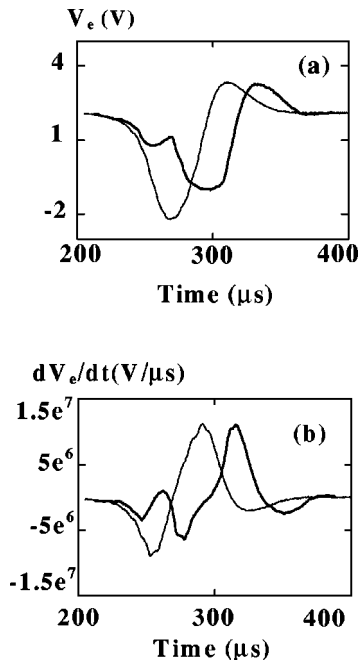
FIG. 5. (a) External signal measured at the volume conductor with (thick line) and without (thin line) ACS. (b) First time derivative of external signal measured at the volume conductor with (thick line) and without (thin line) ACS. Note how the wave form (the signal and its first derivative) is more complex with the ACS.

and 7(b). Signal shape and amplitude depended strongly on the measuring point. Nevertheless, as in previous case, a constant conduction velocity (0.14 circuits/μs) as well as an exceptional delay (26.4 μs) between circuits 21 and 23 were observed. The irregularities in the shape of the external
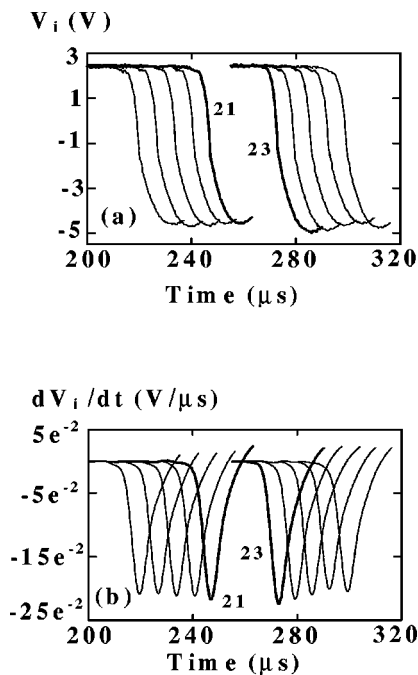

FIG. 6. (a) Depolarization part of the internal signal for circuits near the ACS. (b) First time derivative of depolarization part of internal signal for circuits near the ACS. In this case, the wave shape remains unaltered and only a sudden increase of the delay between consecutive circuits (from 7.0 μs to 25.2 μs) is observed.
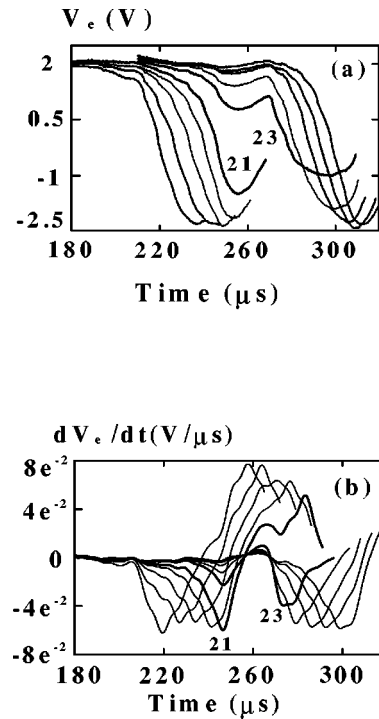

FIG. 7. (a) Depolarization part of external signal for circuits near the ACS. (b) First time derivative of depolarization part of external signal for circuits near the ACS. As in the internal signal, an increase in the delay between consecutive circuits (from 7.0 μs to 26.4 μs) is observed. In addition, the external signal is considerably distorted near the ACS, due to the contribution of different circuits, which arrives at the measuring point with different delays throughout the volume conductor.

wave form for circuits near the ACS are due to the contribution from the sources of the rest of the circuits in the array. In particular, two peaks can be clearly observed for circuits close to the ACS. The main peak corresponds to the local depolarization process, the secondary one to the contribution of the rest of the circuits. This secondary peak was only clearly visible for circuits near the ACS due to the delay in signal propagation induced by R_a. For circuits far from the ACS, the secondary peak was not observed because the large distance to the signal source. Secondary peak appearance can easily be correlated with the presence of the ACS by looking at V_e and dV_e/dt of circuits 21 and 23. Circuit 21 shows the secondary peak after the main peak and circuit 23 presents the secondary peak before the main one. In Fig. 7(b), the minimum of the secondary peak dV_e^{21}/dt (the first circuit before the ACS) occurs with the same LAT of dV_e^{23}/dt (the first circuit after the ACS). Note that only the main peak is propagating through the medium.

The correlation between the LAT corresponding to internal and external measurements was determined by different methods (see Appendix) as shown in Fig. 8. In spite of all methods providing a similar fitting with similar accuracy, the first derivative method has proven to be the most suitable when describing LAT near ACS.

IV. DISCUSSION

Fractionated electrograms of epicardial recordings were associated with disturbances in conduction due to anatomical
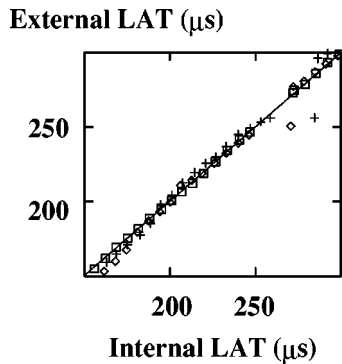
External LAT (μs)

FIG. 8. Correlation between the external and internal LAT measured using zero cross ($+$), minimum of the signal ($\diamond$), and signal first time derivative ($\square$). The straight line with slope 0.995 and an accuracy better than 99.9% was calculated using the third method.

TABLE III. Linear correlation between the internal and external LAT evaluated by different methods.

Method	b	R^2	d_m (μs)
Zero cross	0.995	0.99	23.00
Minimum	0.980	0.98	29.21
First derivative minimum	0.995	0.99	2.67

obstacles and/or effects of the microstructure of the tissue [14,33–35]. There is little experimental work based on this hypothesis because the requirements on measuring systems exceeded by far the performance of available mapping systems concerning resolution in time and space. We recently developed a cardiac micromapping system which allows one to study epicardiac signals with subcellular resolution (20 μm/5 μs) [26].

By means of this system we can record potentials in the volume conductor surrounding the cardiac tissue with a spatio-temporal resolution unknown up to now. However, excitation spread within the tissue cannot be measured directly in microscopic details by this system.

From histological studies we know data about size, contours, and complexity of cardiac cells and their connections in average [9–11,13], but during the electrophysiological experiment no microstructural information about the tissue under examination is available. Superficial obstacles like small vessels (100 μm diameter) sometimes can be detected with a microscope and effects of such intermediate sized discontinuities on extracellular electrograms have been published recently [36]. Coupling structures between cells or groups of cells *in vitro* are not visible optically but their effect could be demonstrated by changing the direction of the excitation spread due to the anisotropy of coupling structures.

From computer simulations with 1D models of excitation spread relating to the continuous cable theory we know about border effects at the ends of the *cable* [29]. The shape of the signal at both ends of the cable changes substantially compared to signals of the middle. Similar changes can be expected at sites where propagating waves collide.

We assume that in cardiac tissue groups of cells are strongly coupled, but are separated from other groups of cells by gradual or complete loss of electrical coupling. Therefore, we could expect piecewise continuous conduction within strongly coupled areas interrupted by discontinuous conduction processes at sites of uncoupling borders. It becomes clear that the complexity of such events in space and time can increase indefinitely, especially if the microstructure was altered by densely placed reduction in coupling structures (like connective tissue in aged hearts). Uncoupling effects are characterized by local delays of the depolarization signal exceeding those expected for the average conduction velocity [37,38].

The complexity of $d\Phi_e/dt$ makes it difficult to follow each signal in space even from recordings from 2D electrode arrays. In order to elucidate the spatio-temporal relationship, we looked at signals of $d\Phi_e/dt$ from linear subsets of electrodes of the 2D array oriented roughly parallel to the direction of propagation. For uniform LP, we found that although local conduction increased towards electrode 5, no abrupt changes in direction or local velocity could be observed [Figs. 4(a) and 4(c)]. It should be noted that the electrode array was not placed exactly at the main axis of LP and not be oriented accurately parallel to the fiber axis of the tissue. These circumstances might account for the continuous increase of local conduction velocity. In contrast to this, in case of discontinuous conduction of TP it was difficult to identify the individual deflections and their spatio-temporal relationship. As can be seen in the isochrone map 1 in Fig. 4(b), substantial irregularities of wave fronts undergoe substantial changes of local conduction velocities (10:1). Within the area under study (shaded), there was no substantial change in direction. From this, we can conclude that the spatio-temporal behavior of signals $E-A$ is based rather on mechanisms like shown in our quasi-2D model than on 2D or even 3D effects. In double deflections, an alternating effect of the dominant amplitudes could be seen following neighboring electrograms recorded along the average direction of propagation direction. Wave 1 represented by the signal 1 in Fig. 4(b), seems to stop at recording site D, where propagation changes to a new carrier wave 2 transporting the cardiac impulse to B. Between B and A a third wave arises. In the vicinity of such a site of discontinuity, two processes can be observed: (1) two deflections of $d\Phi_e/dt$ separated by a local delay appear and (2) one signal undergoes the stopping process and changes to electrotonic behavior (i.e., decreasing amplitude with distance and no change of LAT), while the other one starts to propagate with increasing amplitude. The simplified quasi-2D-hardware model gives an insight to which mechanisms induce such effects.

It should be clearly stated that the model does not reflect the biophysical features of real tissue. Signal shape is different due to the different nature of both media (an array of electronic circuits is a three-variable medium with an excitable fixed point) whose dynamics is much simpler than membrane dynamics. Furthermore, cardiac tissue works in 2D (or even 3D) and our hardware model describes the simplest coupling to show effects of local uncoupling in 1D. Even, if similar effects of discontinuities can be observed in heart tissue, the real situation is much more complex. Fractionation in most cases consists not of two separate events, but of multiple events, which could also have different directions of propagation in 2D or even 3D. Realization of such structures by electronic circuits is far beyond current technical availabilities (it would be necessary to build up at least

400 elements with consequent problems in the number of measuring channels and sampling rate in data acquisition system). Therefore, a future task would be to slow down circuit dynamics in order to apply available low-cost multi-channel recording systems.

Nevertheless, both the *in vitro* experiments and the hardware model share a discretely coupled nature interfaced to a continuous volume conductor. The hardware model allows one to control the coupling at any site by changing the values of coupling resistances, which cannot be achieved in heart tissue. In addition, signals can be measured simultaneously both in active and passive medium.

In summary, the electronic model allows one to control the dynamics of each circuit and the connections among them. This permits one to correlate the internal and external signal, which cannot be easily achieved in cardiac experiments. Thus this model provides an explanation of the fractionated electrocardiograms obtained in transverse propagation.

ACKNOWLEDGMENTS

APPENDIX

A crucial point in the reconstruction of propagation isochrones is the method to determine the LAT. At sites where signals are distorted, there is a substantial difference in results of LAT between measurements from the active and from the passive medium depending on the method. Time of zero crossing, time of the signal minimum and time of the minimum of the signal first derivatives were used. When correlating the external and internal LAT, all methods provided a linear dependence with a slope close to one. The minimum of the first derivative method resulted in the best fit and in the smallest deviation from the fitted line as summarized in Table III, where $d_m = \max_{i=1\ldots30}\{Y_{\text{ext}}^i - a - bX_{\text{int}}^i\}$ is the largest deviation of a single pair of LAT from the fitted straight line. Y_{ext}^i and X_{int}^i represent the external and the internal LAT at circuit i, respectively. It must be taken into account that the time delay between two neighboring circuits is 7.0 μs.

[1] V.I. Krinsky, in *Selforganization. Autowaves and Structures Far from Equilibrium,* edited by V.I. Krinsky (Springer-Verlag, Berlin, 1984), p. 9.

[2] Y. Kuramoto, *Chemical Oscillations, Waves and Turbulence* (Springer-Verlag, Berlin, 1984).

[3] M. Ruiz-Villarreal, M. Gómez-Gesteira, C. Souto, A.P. Muñuzuri, and V. Pérez-Villar, Phys. Rev. E **54**, 2999 (1996); M. Ruiz-Villarreal, M. Gómez-Gesteira, and V. Pérez-Villar, Phys. Rev. Lett. **78**, 779 (1997).

[4] A.P. Muñuzuri, M. Gómez-Gesteira, V. Pérez-Muũzuri, V.I. Krinsky, and V. Pérez-Villar, Phys. Rev. E **48**, 3232 (1993); **50**, 4258 (1994).

[5] J.D. Murray, *Mathematical Biology* (Springer-Verlag, New York, 1989).

[6] *Discretely-Coupled Dynamical Systems*, edited by V. Pérez-Muñuzuri, V. Pérez-Villar, L.O. Chua, and M. Markus (World Scientific, Singapore, 1996).

[7] A.V. Holden, M.J. Poole, and J.V. Tucker, Int. J. Bifurcation Chaos Appl. Sci. Eng. **6**, 1623 (1996).

[8] A.V. Panfilov and A.V. Holden, *Computational Biology of the Heart* (Wiley, Chichester, 1997).

[9] N.J. Severs, Int. J. Cardiol. **26**, 137 (1990).

[10] R.H. Hoyt, M.L. Cohen, and J.E. Saffitz, Circ. Res. **64**, 563 (1989).

[11] G. Gourdie, C.R. Green, and M.J. Severs, J. Cell. Sci. **99**, 41 (1991).

[12] J.E. Shaffitz, R.H. Hoyt, R.A. Luke, H.L. Kanter, and E.C. Beyer, Trends Cardiovasc. Med. **2**, 56 (1992).

[13] M.S. Spach and J.F. Heidlage, Circ. Res. **76**, 366 (1995).

[14] M.A. McGuire, J.M.T. DeBakker, J.T. Vermeulen, T. Opthof, A.E. Becker, and M.J. Jansen, Circulation **84**, 2351 (1994).

[15] P.I. Gardner, P.C. Ursell, J.J. Fenoglio, and A.L. Wit, Circulation **72**, 596 (1985).

[16] A. Kadish and J.F. Spear, Cardiovasc. Res. **28**, 259 (1994).

[17] A.P. Muñuzuri, V. Pérez-Muñuzuri, and V. Pérez-Villar, IEEE Trans. Circuits Syst., I: Fundam. Theory Appl. **40**, 872 (1993).

[18] A.P. Muñuzuri, V. Pérez-Muñuzuri, M. Gómez-Gesteira, L.O. Chua, and V. Pérez-Villar, Int. J. Bifurcation Chaos Appl. Sci. Eng. **5**, 17 (1995).

[19] V. Pérez-Muñuzuri, A.P. Muñuzuri, M. Gómez-Gesteira, V. Pérez-Villar, L. Pivka, and L.O. Chua, Philos. Trans. R. Soc. London, Ser. A **353**, 101 (1995).

[20] V. Pérez-Muñuzuri, M. Gómez-Gesteira, A.P. Muñuzuri, L.O. Chua, and V. Pérez-Villar, Physica D **82**, 195 (1995).

[21] A.P. Muñuzuri, M. deCastro, E. Hofer, V. Pérez-Muñuzuri, M. Gómez-Gesteira, and V. Pérez-Villar, Int. J. Bifurcation Chaos Appl. Sci. Eng. **6**, 1829 (1996).

[22] I. P. Mariño, M. deCastro, V. Pérez-Muñuzuri, M. Gómez-Gesteira, L. O. Chua, and V. Pérez-Villar, IEEE Trans. Circuits Syst., I: Fundam. Theory Appl. **42**, 665 (1995).

[23] M. deCastro, M. Gómez-Gesteira, and V. Pérez-Villar, Phys. Rev. E **57**, 949 (1998).

[24] R.N. Madan, *Chuas Circuit: A Paradigm for Chaos*, World Scientific Series on Nonlinear Science (World Scientific, Singapore, 1993), Series B, Vol. 1, p. 1.

[25] L.O. Chua, Int. J. Elec. Comm. **46**, 250 (1992).

[26] E. Hofer, G. Urban, M.S. Spach, I. Schafferhofer, G. Mohr, and D. Platzer, Am. J. Physiol. **266**, 2136 (1994).

[27] L. Clerc, J. Physiol. (London) **255**, 335 (1976).

[28] M.S. Spach, W.T. Miller III, and E. Miller-Jones, Circ. Res. **45**, 188 (1979).

[29] M.S. Spach and J.M. Kootsey, IEEE Trans. Biomed. Eng. **32**, 743 (1985).

[30] V. Pérez-Muñuzuri, V. Pérez-Villar, and L.O. Chua, Int. J. Bifurcation Chaos Appl. Sci. Eng. **2**, 403 (1992).

[31] J.P. Keener, SIAM (Soc. Ind. Appl. Math.) J. Appl. Math. **47**,

556 (1987); J. Theor. Biol. **148**, 49 (1991).

[32] *Physiology and Biophysics*, edited by T.C. Ruch and H.D. Patton (Saunders, Philadelphia, 1965).

[33] M.S. Spach, J.F. Heidlage, E.R. Darken, E. Hofer, K.H. Raines, and C.F. Starmer, Am. J. Physiol. **266**, 1855 (1992).

[34] W.C. Cole, J.B. Picone, and N. Sperelakis, Biophys. J. **53**, 809 (1988).

[35] W.S. Ellis, D.M. Auslander, and M.D. Lesh, Electrocardiol. **27**, 171 (1994).

[36] E. Hofer, G. Mohr, A.C. Jorge, D. Platzer, and I. Schafferhofer, Int. J. Bifurcation Chaos Appl. Sci. Eng. **6**, 1767 (1996).

[37] V.G. Fast, B.J. Darrow, J.E. Saffitz, and A.G. Kleber, Circ. Res. **79**, 115 (1996).

[38] S. Rohr and B.M. Salzberg, Biophys. J. **67**, 1301 (1994).